 FDMP, vol.10, no.1, pp.63-81, 2014

Simulation of Thermal Fluid-structure Interaction Phenomena in a Liquid Sodium Porous System

Yan Shen[1], Hong Zhang[1,2,3], Hui Xu[1], Tong Bai[1], Ping Yu[1]

Abstract: Single-unit and multi-unit models of porous media (metal felts) have been used to investigate thermal fluid-structure interaction phenomena in a liquid sodium system. Micro-scale aspects have been studied via numerical simulations. The permeability of metal felts has been measured experimentally to verify the reliability of the models used. This integrated approach has allowed a proper evaluation of the interdependencies among phenomena on different scales (including relevant information on skeleton deformation and pressure drop as a function of different parameters). Pressure drop generally increases with velocity and heat flux for both laminar and turbulent flows. The final deformation is greater when turbulence is considered. When the flow is laminar and its rate changes linearly with time, the deformation amount also varies linearly.

Keywords: metal felts, liquid sodium, fluid-structure coupled, pressure drop, deformation, permeability.

Nomenclature

A	area, [m^2]
b	width of porous medium model, [m]
d	fiber diameter, [m]
f	the volume force, [N/m^3]
G	shear modulus, [Pa]
k	thermal conductivity, [W/(m·K)]
K	permeability, [m^2]
l	length, [m]
h	height, [m]
h_{fg}	latent heat, [kJ/kg]

[1] College of Energy Engineering, Nanjing Tech University, Nanjing Jiangsu, PR China
[2] Changzhou Institute of Technology, Changzhou, PR China.
[3] Corresponding Author. Email: hzhang@njtech.edu.cn

m	flow mass, [kg/s]
P	pressure, [Pa]
q	heat flux, [kW/m^2]
t	time, [s]
T	temperature, [K]
u	displacement, [m]
U	velocity, [m/s]
W	input power of the system, [J]

Greek symbols

β	thermal elastic coefficient, [/K]
ε	strain
λ	Lame constants
μ	dynamic viscosity,[Pa·s]
ρ	density,[kg/m^3]
σ	stress,[N/m^2]
Φ	viscous dissipation term
ϕ	porosity

Subscripts

1,2,3,4	cross-section 1, 2, 3 and 4
b-d	sudden expanded cross-section
b-x	sudden reduced cross-section
d	large area in sudden expanded pipe
w	right angle elbow
i,j	equal to 1, 2 and 3, respectively, that is x, y and z
l	fluid
o	initial state
T	temperature
V	volume
x	small area in sudden expanded pipe
z	straight pipe

1 Introduction

Liquid metal flow and heat transfer in porous media have received much attention in the past because of their importance in high temperature heat pipe [Cui et al. (2006)], nuclear power [El-Genk (2008)], space and atomic industries, high or ultra-high temperature cooling [Makhankov (1998)] and other high effective heat exchangers. Metal felts, which are a type of porous medium used in heat pipe, have excellent flow and heat transfer characteristics because their porosity can reach 90% or more, and the minimum diameter of the wire can be 1 μm. On the one hand, the skeleton of metal felt can be deformed by the impact of liquid metal flow, and on the other hand, the deformation of the skeleton can affect the liquid metal flow as well as the thermal performance of porous media. Therefore, microscopic flow and heat transfer are studied in porous media with sodium liquid by considering thermal fluid-structure interaction.

To obtain the hydraulic and thermal characteristics for the complex microstructure of the porous medium-liquid sodium system in heat pipe, an appropriate model is built in micro scale. Most of the models simplify irregular porous media to regular form, such as particle models [Ahmadi et al. (2001); Wittig et al. (2012)], capillary models, statistical models and network models. Particle porous medium is more common in actual production than other models, such as soil, coal, grain and other granular or powder materials. The spheres model was one of the particle models and was developed quickly in theory. Jeong et al. (2008) investigated the thermal dispersion in a porous medium by using the lattice Boltzmann method, including two-dimensional arrays of uniformly distributed circular and square cylinders, and uniformly distributed spherical and cubical inclusions by considering the effect of porosity and the fluid-solid diffusivity ratio. Xu and Jiang (2008) studied numerically the flow characteristics of water and air in particle-level porous media with different average diameters. The capillary model [Yang et al. (2009)] was the most utility pore model and can easily account for permeability, average pore size or pore size distribution, porosity and other structural parameters. The statistical method, inspired by the kinetic theory and quantum theory, is used to describe the chaotic structure of porous media [Sahimi et al. (1990)]. Based on the microscopic seepage physical mechanism, the pore network model is common for the static or dynamic characteristics of fluid flow and heat transfer particularly in inhomogeneous media [Figus et al. (1999), Ahmadi et al. (2001), Part (2010)]. In recent years, three-dimensional imaging technology, such as X-ray computed tomography (CT) and digital image correlation (DIC) techniques, was used in micro structure models of porous media [Wildenschild and Sheppard (2013); Narsilio et al. (2009)]. Fractal theory was also used to examine thermal conductivity and other characteristics [Lv et al. (2006)]. However, fluid-structure interaction was not considered in the micro porous medium studies discussed above.

For many years, considerable attention has been given to fluid-structure interaction in porous media because of its importance in many applications, such as geotechnical and geo-environmental engineering [Gatmiri et al. (2010); Wang et al. (2009); Taron et al. (2009)] and building (Obeid et al. 2001). A number of investigations focused on numerical experiments of thermal-fluid-structure coupling models or computational algorithms based on the average theory [Aouachria (2009); Hamimid et al. (2011)] or the lattice Boltzmann method of porous media [Arab et al. (2006); Derksen (2012); Suga et al. (2009)], but few of them considered the interaction in microscopic porous media. However, metal felt is easily deformed, and the deformation mechanism in micro scale remains unclear. Therefore, the thermal fluid-structure interaction is considered in micro models of porous media with liquid sodium used as a working fluid.

The aim of this paper is to reveal the microscopic fluid-structure interaction of metal felt wick inside high temperature heat pipe. To observe the fluid-structure interaction in micro models, a three-dimensional single-unit model and a multi-unit model of metal felts will be established. The hydraulic parameters of the models will be compared with the experimental data to verify the reliability of the models. This study further explores the details of the fluid flow and deformation mechanism inside metal felts-liquid sodium system and provides a theoretical basis for further development and the application of cooling at high temperature and ultra-high temperature.

2 Physical model

The metal felt wick 08/300 is provided by Bekipor Company from Belgium, where 08 represents the fiber diameter of 8 μm and 300 represents the surface density of 300 g/m^2. The porosity, when measuring metal felt, can reach more than 96%. To make porosity consistent with actual metal felt, the models contain fiber with an 8μm diameter, and the entire single unit cube for the length of a side is 62.5 μm.

In this paper, metal felt wick with numerous fibers is considered an isotropic material. Taking into account the symmetry of the structure and combining the particle model, capillary model and actual feature, a three-dimensional single-unit model and a multi-unit model in micro scale are built as shown in Fig. 1. The simplified porous medium is clear and regular to reveal the fluid-structure interaction in micro scale.

A single-unit model can reflect the fluid-structure microscopic interactions, but the interaction between the units is neglected. Therefore, 27 unit models are combined for a multi-unit model with the length of a side as 187.5 μm.

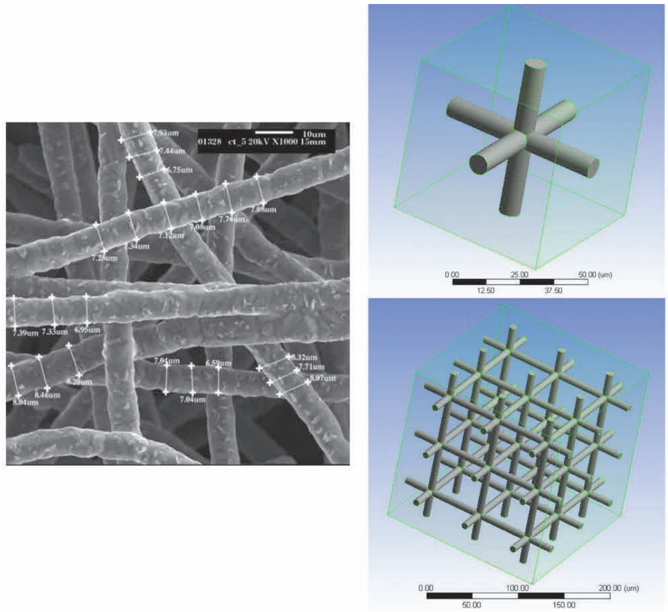

Figure 1: Scheme for metal felt (Moss 2002), single-unit and multi-unit models

3 Mathematical model

3.1 Control equations

This analysis assumes that the porous media is homogeneous and isotropic with constant properties and without gravity effect, and the sodium flow is incompressible due to the short calculational region. The classic continuum assumptions can still be used in the fluid flowing equations, and the Navier-Stokes equations can still predict the fluid behavior in the micron scale pipeline at the low Reynolds number [Pfahler et al. (1989)]. The mathematical model of unsteady-state, three-dimensional fluid-structure interaction in micro porous media is developed.

(1) Thermal structure coupling

Temperature difference causes expansion or contraction of the unit skeleton, thereby generating the stress:

$$\varepsilon_T = \beta(T - T_0) \tag{1}$$

(2)Fluid-structure coupling

$$\sigma_{ij,i} + f_j = 0 \tag{2}$$

$$\varepsilon_{ij} = \frac{1}{2}(u_{i,j} + u_{j,i}) \tag{3}$$

$$\sigma_{ij} = 2G\varepsilon_{ij} + (\lambda\varepsilon_v - \varepsilon_T)\delta_{ij} \tag{4}$$

Incompressible fluid equations:

$$\rho\frac{D\mathbf{U}}{Dt} = \nabla\cdot(\mu\nabla\mathbf{U}) - \nabla P \tag{5}$$

$$\frac{D\rho}{Dt} + \nabla\cdot(\rho\mathbf{U}) = 0 \tag{6}$$

The k-ε turbulence model was used in the numerical calculations for the turbulent flow. The fluid pressure as the external force boundary conditions of Eq. (2)-(4) applies to the structure. The displacement and velocity of the structure node as the boundary conditions of Eq. (5)-(6) applies to the fluid.

(3) Effect of fluid field on temperature field

In the flow of the heat exchange system, the effect of the fluid field on the temperature field should meet the first law of thermodynamics:

$$\rho\frac{De}{Dt} = \rho\frac{DQ}{Dt} - \rho P\frac{DV}{Dt} + \mathbf{\Phi} \tag{7}$$

A temperature change causes a change in the fluid dynamic viscosity, which usually can be corrected by an empirical formula. For the actual parameter conditions, viscous dissipation on the wall has little effect on the convective heat transfer [Jiang and Ren (2001)], and the pressure term representing the thermal expansion work is small. Therefore, the viscous dissipation and pressure term can be neglected.

3.2 Operating conditions

The simulation of fluid-structure interaction in metal felt wick is a transient case. For fibrous material, the Reynolds number is calculated using the following formula:

$$Re = \frac{U_l d\rho_l}{\mu_l} \tag{8}$$

Based on the Reynolds number in pores through experiments, the Darcy flow state is Re <1, and Darcy's law is valid for fluid flows with Reynolds numbers less than one. The Forchheimer flow state is 1∼10 < Re <150, and the post-Forchheimer flow is 150 < Re <300, which shows the status of the non-steady-state laminar flow, and Re > 300 for a turbulent state. In this paper, liquid metal flow in heat pipe wicks is mainly laminar flow.

For high temperature working conditions, the heat transfer amount is quite large, and the flow rate in wicks can be calculated by the heat fluxes of heat pipe.

$$U_l = \frac{q}{h_{fg}\rho_l\phi} \tag{9}$$

According to Eq. (9), the certain relationship of flow velocity and heat flux in wicks is linear.

To make velocities consistent with the actual velocities in metal felt wick, flow velocities of 0.01∼0.03 m/s are in the laminar flow state, and inlet velocities of 0.04∼0.09 m/s are in the turbulent state. The range of Reynolds numbers is from 0.3 to 3.3. The working temperature is approximately 1100 K. The reference pressure of the outlet is 0 Pa. All outside surfaces except the inlet and outlet are in symmetry for the boundary condition. Because wicks are spot welded on the inner wall of the heat pipe, the bottom surface of contacted fiber is set to a fixed surface with no relative displacement. The interaction surface between the fiber and the fluid is set to exchange the load. The models use 316L stainless steel as fiber material and liquid sodium as working fluid and assume that the fiber material is uniform, isotropic and linearly elastic. Khalili et al. (2010) found that the thermal expansion coefficient of the entire porous medium is equal to the solid in the saturated isotropic porous medium. Moreover, the pore size and porosity had no influence on the thermal expansion of the porous medium. Therefore, the thermal expansion coefficient of the solid in Table 1 can be used for the entire porous medium. Detailed properties are shown in Table 1.

Table 1: Solid and fluid physical parameters

Fiber material	316L
Density (kg/m^3)	7980
Young's modulus (GPa)	195
Poisson's ratio	0.3
Thermal expansion coefficient (/K)	16.0×10^{-6}
Fluid	Liquid sodium (1100 K)
Density (kg/m^3)	754.2
Viscosity (Pa·s)	1.64×10^{-4}
Thermal conductivity (W/(m·K))	51.96
Specific heat capacity (J/(kg·K))	1270
Surface tension (N/m)	122.1×10^{-3}

4 Results and discussion

A fluid-structure interaction can be simply divided into a unidirectional and bidirectional coupling. In unidirectional coupling, the fluid field distribution is calculated, and its critical parameters are determined as the load is transmitted into a solid structure without considering the impact of the solid on the fluid, i.e., the boundary of the fluid changed a little and does not affect fluid distribution. Bidirectional coupling takes the affection of both the fluid to solid and solid deformation to fluid field distribution into consideration. The final equilibrium state is obtained by the interaction convergence of the solid and fluid. Thermal-structural coupling is a common unidirectional coupling, and fluid-structure coupling can be solved by unidirectional or bidirectional coupling simulation based on the deformation size.

In this paper, bidirectional coupling is used, and the simulation results and their analyses are as follows:

4.1 Pressure drops change with flow velocities

Pressure drops change with flow velocities and heat fluxes in laminar and turbulent flow as shown in Fig. 2. The pressure drop increases linearly as the flow velocity increases in laminar flow, which is consistent with Darcy's law. Therefore, Darcy's law is still valid in micro scale. Because the velocities are small in simulations, the effects of inertial forces are not obviously reflected, and the flow velocity and pressure drop has only a small non-linear relationship in turbulent flow.

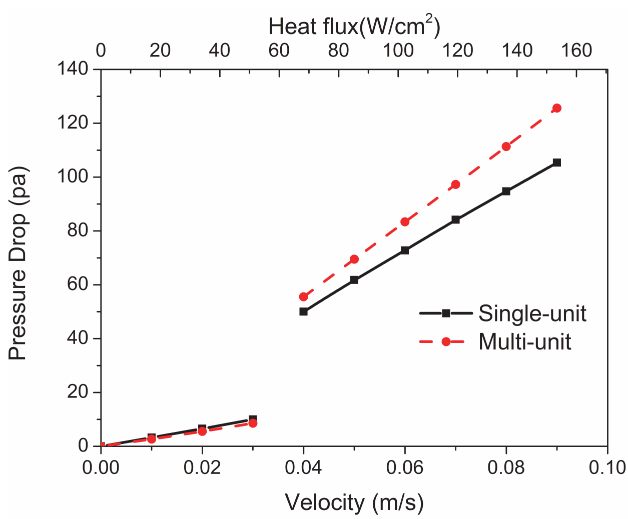

Figure 2: Pressure drops change with flow velocities

The porous medium velocity is uneven as the heat flux changes. The variation of pressure drop in laminar and turbulent flow is similar in a single-unit model and a multi-unit model. Due to the larger fluid field in a multi-unit model, the pressure drop significantly increases in turbulence and is larger than in a single-unit model.

4.2 Skeleton deformation changes with velocities

The highest point in the middle of the flow duct is selected as the monitoring point to obtain the maximum displacement in both the single-unit and multi-unit models. As shown in Fig. 3, the displacement increases as the flow velocities and heat fluxes increase in two models. The maximum amount of deformation in a multi-unit model is much larger than a single-unit model. Thus, the displacement is greatly influenced by the distance from the fixed end to the monitoring point of the metal fiber.

When liquid metal flows within the metal felt wick of a heat pipe, the displacement of the upper wick structure, which is close to the steam flow area, is larger than the bottom wick, and the pore size of the upper metal felt changes and affects the capillary force and liquid evaporation. Therefore, a screen mesh with a large mesh number is used to press the metal felt for supporting and fixing.

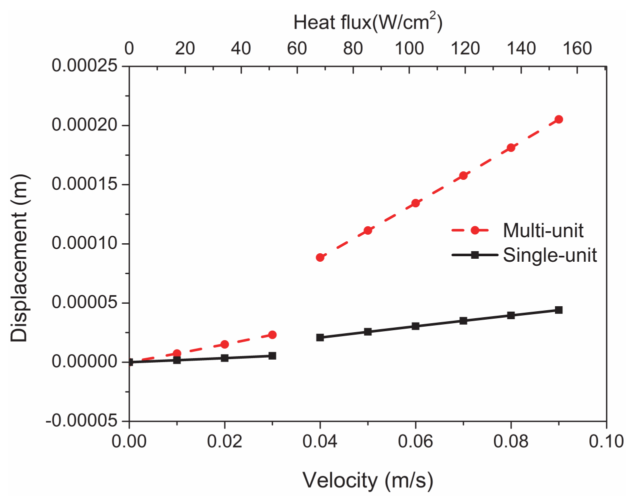

Figure 3: Skeleton deformations change with flow velocities

The deformation amount of a single-unit and a multi-unit model for a variable flow rate is shown in Fig. 4. When the flow rate changes linearly with time in laminar flow, the deformation amount varies linearly, which is different for the initial velocity and slope. The initial speed determines the initial amount of deformation, and the slope affects the rate of deformation change. Variable heat flux in a heat pipe results in flow rate and deformation changes in the metal felt wick. Therefore, a rapid change in heat flux will have a greater impact on the skeleton of metal felt and requires more attention for the operation of a heat pipe.

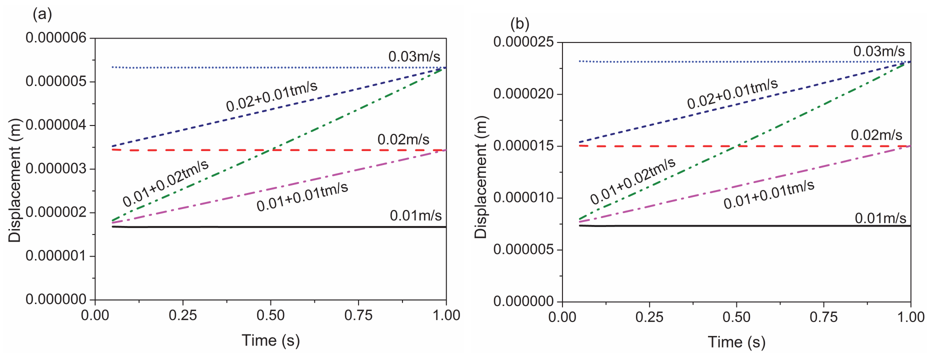

Figure 4: Skeleton deformations change with variable flow velocities (a) single-unit and (b) multi-unit

4.3 Instantaneous skeleton deformation

As shown in Fig. 5(a), the maximum deformation occurs when metal fiber contacts the laminar flow of 0.02 m/s. By considering the fluid-structure interaction, the deformation decreases rapidly, slightly increases and then gradually becomes constant. When the turbulent flow rate is 0.04 m/s, the fluctuation range of skeleton deformation is greater and more intense than laminar flow, and the amount of displacement in the direction of flow is constant and is much larger after a lengthy fluctuation as shown in Fig. 5(b). The spring back value of fiber is small in laminar flow and maintains a small amount of deformation, while the spring back value of fiber is large in turbulent flow and causes a large amount of deformation. Therefore, a clear fluid-structure interaction phenomenon in micro porous media by numerical simulation exists.

A momentary elastic strain response is first produced in the porous medium after loading stress, and then the response may become a continuous viscous strain for a very long time until it finally stabilizes. The elastic strain response can be recovered while the viscous strain response cannot be recovered, and will cause a permanent deformation in the porous medium. The elastic strain response is considered to be instantaneous because the velocity of the stress wave propagation is very large relative to the speed of the stress and the viscous fluid applied. In the micro scale case, the elastic strain is deformed for the porous media, and the process of displacement

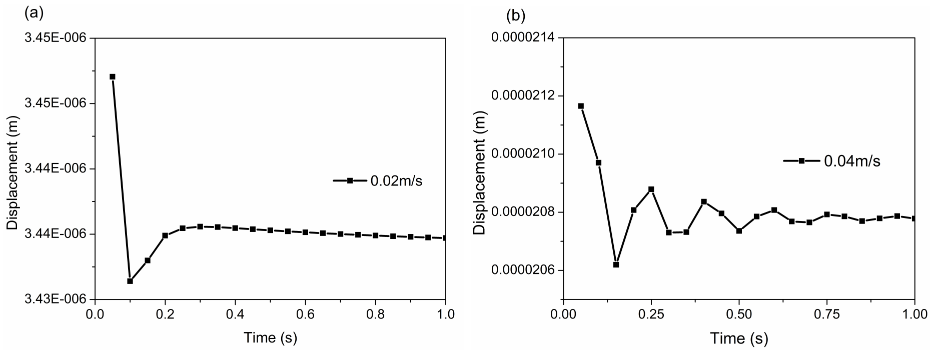

Figure 5: Skeleton deformations change over time in laminar flow (a) and turbulence (b)

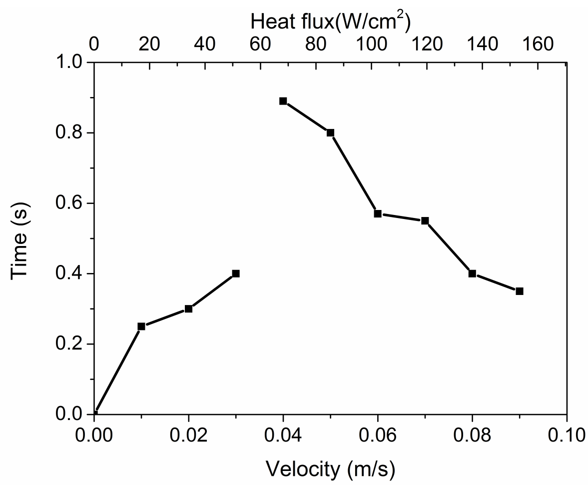

Figure 6: Fluctuation time for different velocities and heat fluxes

fluctuations by the fluid-structure coupling is very short as shown in Fig. 6. The fluctuation time increases in laminar flow and decreases in turbulence, while the flow velocities and heat fluxes increase.

The skeleton deformation changes over time in a single-unit model as shown in Fig. 7. The deformation amount in turbulence is significantly larger than in laminar flow because of the greater perturbation and fluid-structure interaction for a larger flow rate. The flow rate has a great impact on the final deformation amount of the skeleton.

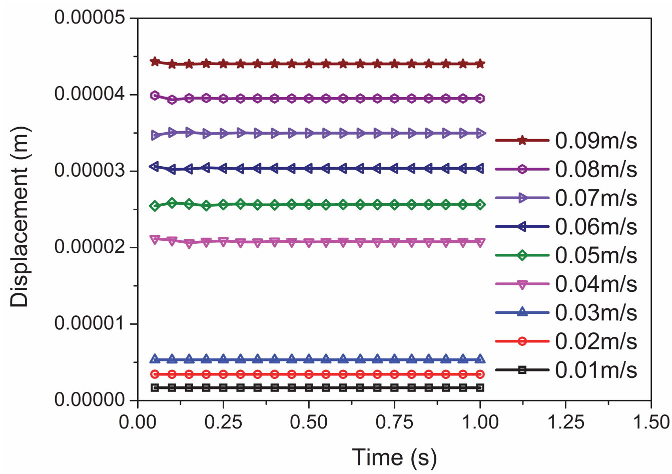

Figure 7: Skeleton deformations in a single-unit model

4.4 *Metal fiber stress distribution*

The stress contour in a single-unit model and a multi-unit model is shown in Fig. 8. Because the association between the units is ignored in a single-unit model, the stress concentration occurs in the junction of the fixed end and in the junction of fibers in a multi-unit model. According to the actual situation, metal felt is formed by compression, and the fibers are in contact with each other but are not fixed. Consequently the stress concentration in actual metal felt will not occur between the junction with fibers, but for the connecting point between the fiber and the heat pipe wall because metal felt is spot welded in the inner wall of a heat pipe.

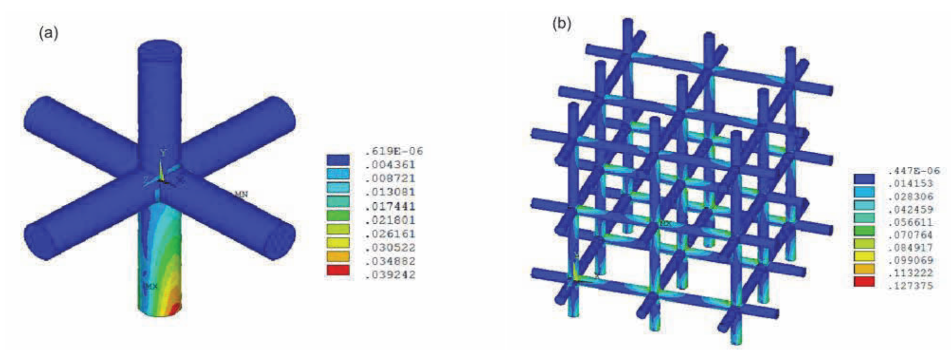

Figure 8: Skeleton stress contour of 0.09 m/s in a single-unit (a) and a multi-unit (b)

5 Experimental verification

The test system consists of the reservoir, metal felt wicks, electronic balance, pipeline and its subsidiaries as shown in Fig. 9. The metal felt in this test has the fiber diameter of 8 μm and the porosity of 96%. The reservoir is a stainless s-teel cylinder with a height of 200 mm, a thickness of 10 mm and a bottom diameter ϕ180 mm. The size of all stainless steel pipelines used in the system is $\phi 8\times2$ mm, and the pipes are connected through a stainless steel right-angle connector. During the experiment, the reservoir is continuously filled with water to maintain the liquid level at a certain height. The height difference is adjusted between the reservoir and the wick through a height adjustable pipe to provide the inlet pressure of the water. The inlet flow rates of water in the tests are 0.005 m/s, 0.006 m/s and 0.010 m/s, respectively in the laminar flow state at an ambient temperature of 283 K.

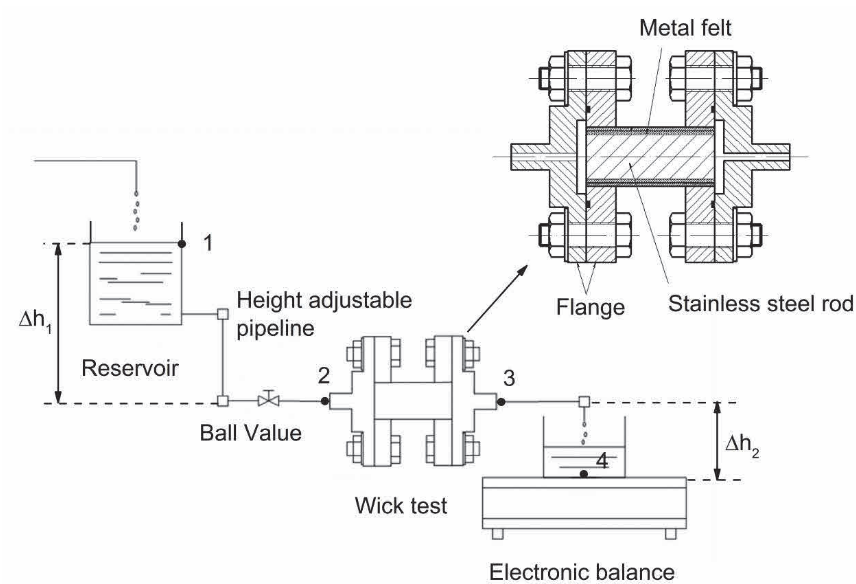

Figure 9: Permeability test system of metal felt wick

Bernoulli's equation of incompressible viscous fluid steady flow is

$$P_1+\rho gh_1+\frac{1}{2}\rho U_1^2+W=P_2+\rho gh_2+\frac{1}{2}\rho U_2^2+\sum h_f \tag{10}$$

To obtain the pressure drop of fluid flowing through the wick, the input and output pressure of the wick are analyzed. As shown in Fig. 9, the cross-sections 1, 2, 3 and

4 are reference areas, and the wick inlet pressure (P_2) and wick outlet pressure (P_3) can be calculated by Eq. (11) and (12). The bottom area of the reservoir is much greater than the cross-sectional area of the pipeline. Therefore, the assumption is that $u_1 \approx 0$, $P_1 = P_4 = P_0$, and P_0 is the atmospheric pressure.

$$P_2 = P_1 + \rho g \Delta h_1 - \frac{1}{2}\rho U_2^2 - \sum h_{f1-2} \tag{11}$$

$$P_3 = P_4 - \rho g \Delta h_2 + \sum h_{f3-4} \tag{12}$$

$$\Delta P = P_2 - P_3 = \rho g\left(\Delta h_1 + \Delta h_2\right) - \frac{1}{2}\rho U_2^2 - \sum h_{f1-2} - \sum h_{f3-4} \tag{13}$$

The parts of the flow pressure loss are as follows:

$$\sum h_z = \frac{32}{Re}\rho U^2 \frac{l}{d} \tag{14}$$

$$\sum h_{b-x} = \frac{1}{2}\left\{0.4\left[1 - \left(\frac{A_x}{A_d}\right)^2\right]\right\}\rho U^2 \tag{15}$$

$$\sum h_{b-d} = \frac{1}{2}\left(1 - \frac{A_x}{A_d}\right)^2 \rho U^2 \tag{16}$$

$$\sum h_w = \frac{0.8}{2}\rho U^2 \tag{17}$$

The term Δh_2 is fixed as shown in Fig. 9. Therefore, the wick pressure difference between the inlet and outlet can be changed by adjusting the height Δh_1 in this experiment.

Water is added into the reservoir continuously to maintain a certain liquid height. The pressure head of the inlet in the metal felt wick is provided and controlled by a height-adjustable pipe to ensure the flow in the wick is in the laminar flow state. The mass of the water in the beaker is recorded with an electronic balance along with the corresponding time of the flow passing through the test section of the wicks.

The deformation of the metal felt in the micro porous media is related to its hydraulic characteristics. Fibers are not consolidated but are staggered together. The change of each fiber will affect the other fibers. Therefore, the connection used in the simulation for the metal felt wick is reasonable. The force in the direction of the fluid flow is as similar as the fluid impaction in these models. Therefore, this simulation can provide some reference for the fluid flow and the deformation in microscopic porous media.

The error of the test comes mainly from the various parameters measured. To obtain the permeability of the metal felt wick, the measured parameters are the length of a wick and the water mass in a certain period of flowing time and flow time. The error can be calculated using the following formula.

$$E(X) \leq \sqrt{\sum \left(\frac{\partial X}{\partial x_i} dx_i \right)^2} \tag{18}$$

For permeability, the relative error is

$$E(K) = \sqrt{\left(\frac{\partial K}{\partial m} dm \right)^2 + \left(\frac{\partial K}{\partial l} dl \right)^2 + \left(\frac{\partial K}{\partial t} dt \right)^2} \tag{19}$$

$$\frac{E(K)}{K} = \sqrt{\left(\frac{dm}{m} \right)^2 + \left(\frac{dl}{l} \right)^2 + \left(\frac{dt}{t} \right)^2} \tag{20}$$

where *dm*, *dl* and *dt*, represent the maximum error of the water mass, the wick length and the fluid flow time, respectively. If *dm* = 0.01 kg, *dl* = 0.5 mm and *dt* = 1 s, the fluid mass range measured in the test is 1$\sim$3 kg, the total length of pipes and wick are in the range of 64$\sim$900 mm, and the fluid flow time is in the range of 231$\sim$699 s, respectively. Therefore, the maximum relative error of permeability values through this testing system is 3.3%.

The fluid pressure drops increased as the flow rates in laminar and turbulent flow increased as shown in Fig. 10, and the macro experimental results have the same tend as the micro simulated results.

Many methods are used to obtain the permeability of porous media (Pereira et al. 2012). Darcy's law is one such method for computing permeability (Williams and Harris 2003). The flow rate and pressure drop through the same porous media structure have a linear relationship in laminar flow. Therefore, the permeability of the structure can be obtained by the mass rate and pressure drop.

$$K = \frac{m \mu_l l}{\rho_l \Delta p A_w} \tag{21}$$

The experimental values that were measured in the test and simulation results for the permeability of the metal felt wick are compared as shown in Fig. 11. To verify the correctness of the permeability, the permeability was tested at three different flow rates. The results show that the permeabilities are nearly consistent for different flow rates. Therefore, the average of the permeabilities is the actual permeability of the metal felt. The permeability of the three-dimensional multi-unit model is consistent with the experimental values but is smaller in the single-unit model, which confirms that the microscopic multi-unit model is more reliable because the unit interaction is ignored in a single-unit model.

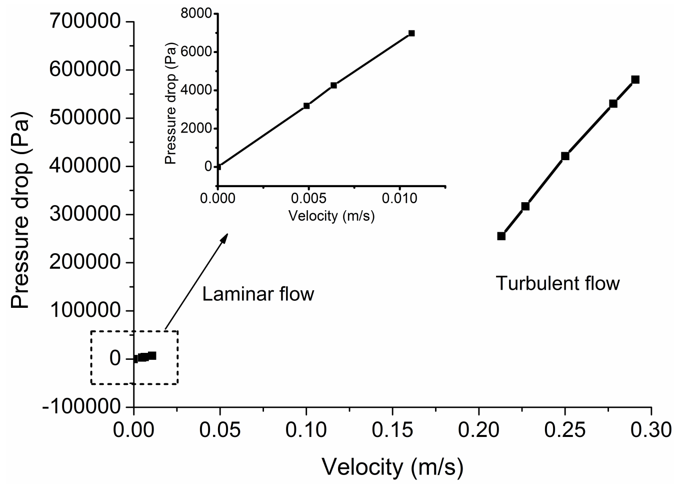

Figure 10: Pressure drops change with flow velocities in test

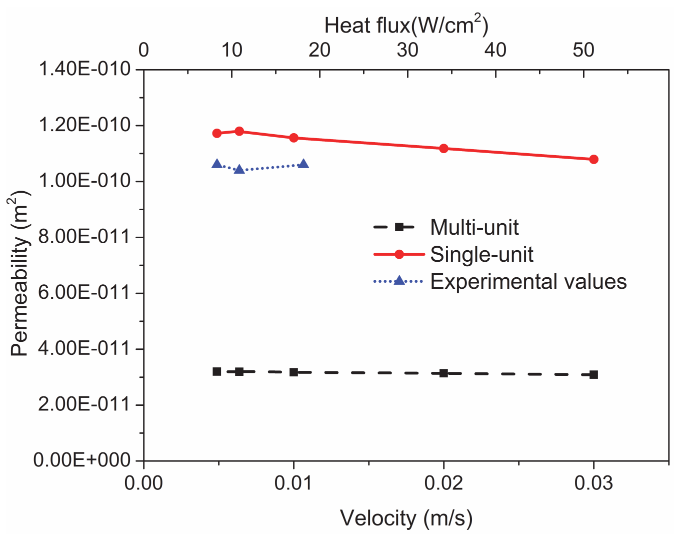

Figure 11: The comparison between experimental values and the simulation results of permeability

6 Conclusion

In this paper, a three-dimensional microscopic single-unit model and a multi-unit model of metal felt wick were built and simulated by considering the fluid-structure interaction in laminar and turbulent flow. The pressure drops increase linearly as the flow velocity increase in these models in laminar flow, which is consistent with Darcy's law. Therefore, Darcy's law can be used in microscopic models. The deformation amount of the skeleton in wicks increases as the flow rate increases. The maximum displacement in a multi-unit model is significantly increased compared with a single-unit model. When the flow rate changes linearly with time in laminar flow, the deformation amount varies linearly, which is affected by the initial velocity and slope. The metal fiber deformation and fluid-structure interaction phenomena are simulated in both a single-unit model and a multi-unit model. The permeability of the three-dimensional multi-unit model is consistent with the experimental values and confirms that the microscopic multi-unit model is more reliable.

Acknowledgement: This article has been supported by the National Natural Science Foundation of China (51076062).

References

Ahmadi, A.; Aigueperse, A.; Quintard, M. (2001): Calculation of the effective properties describing active dispersion in porous media: from simple to complex unit cells. *Advances in Water Resources*, vol. 24, no. 3-4, pp. 423-438.

Aouachria, Z. (2009): Heat and Mass Transfer Along of a Vertical Wall by Natural convection in Porous Media. *FDMP: Fluid Dyn. Mater. Process.*, vol. 5, no. 2, pp.137-148.

Arab, M. R.; Semma, E.; Pateyron, B.; Ganaoui, M. El. (2009): Determination of physical properties of porous materials by a lattice Boltzmann approach. *FDMP: Fluid Dyn. Mater. Process.*, vol. 5, no. 2, pp. 161-176.

Cui, H.; Wang, Z.; Guo, Y.; Xu, W.; Yuan, X. (2006): Thermal performance analysis on unit tube for heat pipe receiver. *Solar Energy*, vol. 80, no. 7, pp. 875-882

Derksen, J. J. (2012): Dense suspensions - solid-liquid interactions at the particle scale. *Progress in Computational Fluid Dynamics*, vol. 12, no. 2-3, pp. 103-111.

El-Genk, M. S. (2008): Space nuclear reactor power system concepts with static and dynamic energy conversion. *Energy Conversion and Management*, vol. 49, no. 3, pp. 402-411.

Figus, C.; Bray, Y. L.; Bories, S.; Part, M. (1999): Heat and mass transfer with phase change in a porous structure partially heated: continuum model and pore network simulations. *International Journal of Heat and Mass Transfer*, vol. 42, no. 14, pp. 2557-2569.

Gatmiri, B.; Maghoul, P.; Duhamel, D. (2010): Two-dimensional transient thermo-hydro-mechanical fundamental solutions of multiphase porous media in frequency and time domains. *International Journal of Solids and Structures*, vol. 47, no. 5, pp. 595-610.

Hamimid, S.; Guellal, M.; Amroune, A.; Zeraibi, N. (2011): Effect of a Porous Layer on the Flow Structure and Heat Transfer in a Square Cavity. *Fluid Dynamics and Materials Processing*, vol. 8, no. 1, pp. 69-90.

Jeong, N.; Choi, D.H.; Lin, C.-L. (2008): Estimation of thermal and mass diffusivity in a porous medium of complex structure using a lattice Boltzmann method. *International Journal of Heat and Mass Transfer*, vol. 51, no. 15-16, pp. 3913-3923.

Jiang, P.-X.; Ren Z.-P. (2001): Numerical investigation of forced convection heat transfer in porous media using a thermal non-equilibrium model. *International Journal of Heat and Fluid Flow*, vol. 22, no. 1, pp. 102-110.

Khalili, N.; Uchaipichat, A.; Javadi, A.A. (2010): Skeletal thermal expansion coefficient and thermo-hydro-mechanical constitutive relations for saturated homogeneous porous media. *Mechanics of Materials*, vol. 42, no. 6, pp. 593-598.

Lv, Y.-G.; Huai, X.-L.; Wang, W.-W. (2006): Study on the effect of micro geometric structure on heat conduction in porous media subjected to pulse laser. *Chemical Engineering Science*, vol. 61, no. 17, pp. 5717-5725

Makhankov, A.; Anisimov, A.; Arakelov, A.; Gekov, A.; Jablokov, N.; Yuditskiy, V.; Kirillov, I.; Komarov, V.; Mazul, I.; Ogorodnikov, A.; Popov, A. (1998): Liquid metal heat pipes for fusion application. *Fusion Engineering and Design*, vol. 42, no. 1-4, pp. 373-379

Moss, T. A. (2002): Building, testing and post test analysis of durability heat pipe #6, SAND2002-0730, Albuquerque: Sandia National Laboratories. pp.1-43.

Narsilio, G. A.; Buzzi, O.; Fityus, S.; Yun, T. S.; Smith, D. W. (2009): Upscaling of Navier–Stokes equations in porous media: Theoretical, numerical and experimental approach. *Computers and Geotechnics*, vol. 36, no. 7, pp. 1200-1206.

Obeid, W.; Mounajed, G.; Alliche, A. (2001): Mathematical formulation of thermo-hygro-mechanical coupling problem in non-saturated porous media. *Computer Methods in Applied Mechanics and Engineering*, vol. 190, no. 39, pp. 5105-5122.

Part, M. (2010): Pore network models for the study of transfers in the porous wick of loop heat pipe. *Heat Pipe Science and Technology*, vol.1, no.2, pp. 129-149.

Pereira, G. G.; Dupuy, P. M.; Cleary, P. W.; Delaney, G. W.(2012): Comparison of permeability of model porous media between SPH and LB. *Progress in Computational Fluid Dynamics*, vol. 12, no. 2-3, pp. 176-186.

Pfahler, J.; Harley, J.; Bau, H.; Zemel, J. (1989): Liquid transport in micron and submicron channels. *Sensors and Actuators A: Physical*, vol. 22, no. 1-3, pp. 431-434.

Sahimi, M.; Gavalas, G. R.; Tsotsis, T. T. (1990): Statistical and continuum models of fluid-solid reactions in porous media. *Chemical Engineering Science*, vol. 45, no. 6, pp. 1443-1502.

Suga, K.;Tanaka, T.;Nishio, Y.; Murata, M. (2009): A boundary reconstruction scheme for lattice Boltzmann flow simulation in porous media. *Progress in Computational Fluid Dynamics*, vol. 9, no. 3-5, pp. 201-207.

Taron, J.; Elsworth, D.; Min, K.-B. (2009): Numerical simulation of thermal-hydrologic-mechanical-chemical processes in deformable, fractured porous media. *International Journal of Rock Mechanics and Mining Sciences*, vol. 46, no. 5, pp. 842-854.

Wang, W.; Kosakowski, G.; Kolditz, O. (2009): A parallel finite element scheme for thermo-hydro-mechanical (THM) coupled problems in porous media. *Computers & Geosciences*, vol. 35, no. 8, pp. 1631-1641.

Wildenschild, D.; Sheppard, A. P. (2013): X-ray imaging and analysis techniques for quantifying pore-scale structure and processes in subsurface porous medium systems. *Advances in Water Resources*, vol. 51, pp. 217-246.

Williams, R. R.; Harris, D. K. (2003): Cross-plane and in-plane porous properties measurements of thin metal felts: applications in heat pipes. *Experimental Thermal and Fluid Science*, vol. 27, no. 3, pp. 227-235.

Wittig, K.; Golia, A.; Nikrityuk, P. A.(2012): 3D numerical study on the influence of particle porosity on heat and fluid flow. *Progress in Computational Fluid Dynamics*, vol. 12, no. 2-3, pp. 207-219.

Xu, R.-N.; Jiang, P.-X. (2008): Numerical simulation of fluid flow in microporous media. *International Journal of Heat and Fluid Flow*, vol. 29, no. 5, pp. 1447-1455.

Yang, D.; Currier, R. P.; Zhang, D. Z. (2009): Ensemble phase averaged equations for multiphase flows in porous media. Part 1: The bundle-of-tubes model. *International Journal of Multiphase Flow*, vol. 35, no. 7, pp. 628-639.